Journal of Solid State Chemistry 182 (2009) 532–537

Contents lists available at ScienceDirect

Journal of Solid State Chemistry

journal homepage: www.elsevier.com/locate/jssc

Preparation, structural and magnetic characterization of $DyCrMnO_5$

M.J. Martínez-Lope, M. Retuerto *, M. García-Hernández, J.A. Alonso

Instituto de Ciencia de Materiales de Madrid, CSIC, Cantoblanco, E-28049 Madrid, Spain

ARTICLE INFO

Article history:
Received 30 July 2008
Received in revised form
6 November 2008
Accepted 16 November 2008
Available online 3 December 2008

Keywords:
RMn_2O_5
Multiferroic oxides
Magnetoelectric
High pressure
Neutron scattering

ABSTRACT

The title compound has been first synthesized by a citrate technique followed by thermal treatments under moderate oxygen pressure conditions, and characterized by X-ray and neutron powder diffraction (NPD) and magnetization measurements. The crystal structure of $DyCrMnO_5$ has been refined from NPD data in the space group *Pbam*; $a = 7.2617(6)$ Å, $b = 8.5161(6)$ Å, and $c = 5.7126(5)$ Å at 295 K. This oxide is isostructural with RMn_2O_5 oxides (R = rare earths) and it contains infinite chains of $(Cr, Mn)^{4+}O_6$ octahedra-sharing edges, linked together by $(Mn, Cr)^{3+}O_5$ pyramids and DyO_8 units. The high degree of antisite disordering exhibited by $DyCrMnO_5$ is noteworthy. The octahedral positions are occupied by roughly 50% of Mn and Cr cations, and the pyramidal groups contain two thirds of Mn and one third of Cr cations. We assume that Mn and Cr cations at the octahedral positions exhibit a tetravalent oxidation state, whereas the metals at the pyramidal positions are trivalent, in order to preserve the electroneutrality of this oxide. The susceptibility vs temperature curve of $DyCrMnO_5$ does not suggest the establishment of a long-range magnetic structure even at low temperatures; the NPD technique does not provide any signal of magnetic ordering, since the reflections do not show any magnetic contribution.

1. Introduction

Magnetoelectric materials are systems where electric and magnetic properties are coupled together [1]. In these materials, magnetization is induced by an electric field or spontaneous polarization is induced by a magnetic field. Consequently, there are interactions between the ferroelectric and magnetic properties. Recently, numerous investigations have been focused on the magnetoelectric RMn_2O_5 (R = rare earth) materials [2–4] and it is shown that the dielectric anomaly observed in RMn_2O_5 is due to lattice effects [5]. These materials possess ferroelectric properties and show antiferromagnetic ordering in the low-temperature region, $T < 30$ K. Especially, the YMn_2O_5 oxide shows dielectric constant anomalies at 19 and 39 K [6].

The crystal structure of RMn_2O_5 is orthorhombic (space group *Pbam*); it is attractive because it contains two crystallographic sites for Mn atoms, with different oxygen coordinations and oxidation states. The Mn^{4+} ions are located at the 4*f* sites, octahedrally coordinated to oxygens, whereas Mn^{+3} ions occupy the 4*h* sites and they are bonded by five oxygens, forming a distorted tetragonal pyramid [7–9]. These oxides exhibit complex, incommensurate magnetic structures defined by the propagation vector $k(1/2, 0, k_z)$ where the value of k_z depends on the type of R [10,11]. In $LaMn_2O_5$ the magnetic structure is commensurate with $k(0, 0, 1/2)$ [12]. (Ho, Tb, Er, Y)Mn_2O_5 oxides [2] present a magnetic transition to a commensurate structure at the ferroelectric transition temperature T_C. One of the disadvantages of these compounds is the low temperature at which the magnetoelectric phenomenon appears, so it seems to be necessary to search for new related oxides that could present this behavior at higher temperatures.

With the aim of inducing new magnetic interactions in the members of the RMn_2O_5 family, we recently designed and prepared $RFeMnO_5$ (R = Y, Ho, Er) [13–15] and $YCrMnO_5$ [16] oxides, which are obtained by replacing Mn^{3+} by Fe^{3+} and Cr^{3+}, respectively. In this paper we report on the preparation of a new material of stoichiometry $DyCrMnO_5$, isostructural with the RMn_2O_5 compounds and obtained by substitution of Cr by Mn cations. This oxide must be prepared under moderate O_2 pressure, and it has been characterized from the structural point of view from neutron powder diffraction (NPD) data, complemented with macroscopic magnetic susceptibility measurements.

2. Experimental section

Polycrystalline $DyCrMnO_5$ was prepared by a wet chemistry procedure involving the formation of citrate precursors. Dy_2O_3, $Cr(NO_3)_3 \cdot 9H_2O$ and $MnCO_3$ in stoichometric proportion were dissolved in a saturated citric acid solution. By gently heating the solution was slowly evaporated, leading to an organic resin. After dying the resin at 120 °C, it was slowly decomposed at temperatures up to 600 °C in air, thus eliminating the organic matter. Subsequent high-oxygen-pressure treatments

* Corresponding author. Fax: +34 91 372 06 23.
E-mail address: mretuerto@icmm.csic.es (M. Retuerto).

0022-4596/$ - see front matter © 2008 Elsevier Inc. All rights reserved.
doi:10.1016/j.jssc.2008.11.023

were performed in a VAS furnace. About 2 g of the precursor powder was contained in a gold sample holder during the oxygenation process. The sample was slowly heated up to 900 °C at a final pressure of 42 bar and held at this temperature for 12 h. The product was finally cooled, under pressure, at 300 °C h^{-1} down to room temperature. Finally, the oxygen pressure was slowly released.

Neutron powder diffraction diagrams were collected using the high-resolution HRPT diffractometer of the SINQ spallation source, at the Paul Scherrer Institute, Villigen, Switzerland. The sample, weighing 2 g, was packed in a cylindrical vanadium holder of 6 mm diameter. The room temperature pattern was collected with a wavelength of 1.494 Å. Then the sample was cooled down in an orange cryostat, and one pattern was obtained at 5 K with a wavelength of 1.886 Å. In all cases the high-intensity mode was used; the collection time was 4 h per diagram. A double-walled vanadium sample holder was employed to minimize absorption. The neutron diffraction patterns were analyzed with the Rietveld method [17], using the FULLPROF program [18]. For the refinement of the profile, a pseudo-Voigt function was used to simulate the peak shape, and the background was fitted with a fifth-degree polynomial function. The coherent scattering lengths for Dy, Cr, Mn, and O were, 16.9, 3.635, −3.73, and 5.803 fm, respectively. In the final run the following parameters were refined: background coefficients, zero point, half width, pseudo-Voigt and asymmetry parameters for the peak shape; scale factor, positional and thermal factors, and unit-cell parameters.

The magnetic measurements were performed in a commercial SQUID magnetometer from Quantum Design. The *dc* magnetic susceptibility was measured both in zero-field cooling (ZFC) and field cooling (FC) conditions in the temperature intervals $1.8\,K < T < 400\,K$, respectively, under a magnetic field of 1 kOe. As regarding the isothermal magnetization curves, different hysteresis cycles were obtained at $T = 3$, 50, 100, and 300 K and for a magnetic field ranging from −50 to 50 kOe.

3. Results

3.1. Preparation

The synthesis of $DyCrMnO_5$, obtained as a dark brown polycrystalline powder, requires oxidizing conditions in order to reach the tetravalent oxidation states of Mn and Cr. This is achieved under moderate O_2 pressures; the departure of very reactive citrate precursors is also essential to isolate the wanted single-phase material, since the oxygenation process and the formation of the complex oxide is favored by the use of reactive, finely divided, and homogeneous precursors. The presence of the competitive $DyMnO_3$ perovskite, nominally containing Mn^{3+}, was eliminated in the thermal treatments under O_2 pressure. The final O_2 pressure is an important parameter, which was tuned after several unsuccessful trials: treatments at O_2 pressures at 42 bar led to a pure $DyCrMnO_5$ phase, whereas at higher pressures the competitive phase $DyCrO_4$ stabilized, containing Cr^{5+}. Fig. 1 shows the X-ray diffraction (XRD) pattern of $DyCrMnO_5$. It can be indexed in an orthorhombic unit cell, isotypic to that of RMn_2O_5, with no additional peaks that could indicate the presence of superstructures or departure of the mentioned symmetry.

3.2. Crystallographic structure from neutron and X-ray powder diffraction

A combined refinement of the crystal structure from NPD and XRD data was carried out in the orthorhombic space group *Pbam*

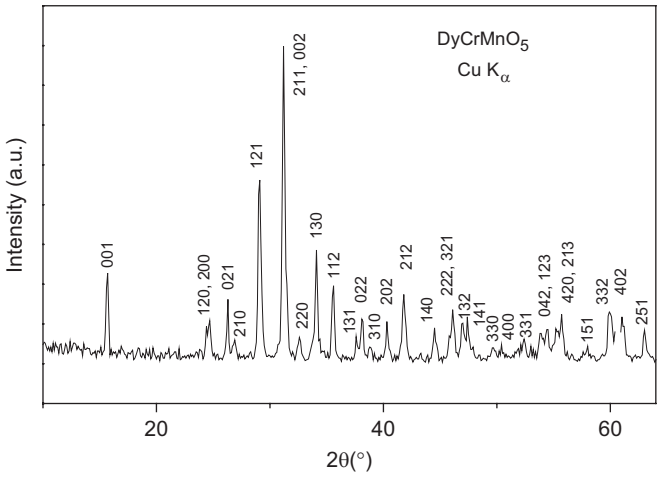

Fig. 1. XRD pattern of $DyCrMnO_5$, indexed in an orthorhombic unit cell with parameters $a = 7.2619(6)$ Å, $b = 8.5163(6)$ Å, and $c = 5.7128(5)$ Å.

(No. 55), with unit-cell parameters $a = 7.2619(6)$ Å, $b = 8.5163(6)$ Å, and $c = 5.7128(5)$ Å. The crystal structure of $YCrMnO_5$ was used as the starting model [16]. Dy atoms were placed at 4*g* $(x,y,0)$ positions, Mn at 4*f* $(0,1/2,z)$ sites, Cr at 4*h* $(x,y,1/2)$, and the four crystallographically independent oxygen atoms at 4*e* $(0,0,z)$, 4*g*, 4*h*, and 8*i* (x,y,z) positions. This ideal atomic distribution gave rise to an unsatisfactory agreement between the calculated and observed patterns. The presence of antisite disorder between Cr and Mn cations was then checked; the refinement considerably improved, reaching a R_{Bragg} of 5.98%. In fact, we found an extremely important degree of antisite disordering in this sample, as shown in Table 2. Additionally, the partial occupancy of Cr/Mn at 4*h* and 4*f* positions was decoupled in the final refinement, allowing the independent refinement of the occupancy factor at both sites: by doing so, the final refined stoichiometry was somewhat apart from the nominal Cr/Mn = 1/1 composition, but the quality of the final refinement warrants the validity of this result. The refined crystallographic formula can be written as $Dy[Mn_{0.44(1)}Cr_{0.56(1)}]_{4f}[Cr_{0.38(1)}Mn_{0.62(1)}]_{4h}O_5$, which corresponds to an empirical formula $DyMn_{1.06(1)}Cr_{0.94(1)}O_5$. It is worth underlining that the refinement of the mixed occupancy factors of Cr and Mn over the same crystallographic site, which would be unfeasible by XRD, is very precise by neutron diffraction given the opposite values of the scattering lengths for Cr (3.635 fm) and Mn (−3.73 fm). By the same reason, and given the comparable amount of Cr and Mn found in both sites, the average scattering length at both positions is very weak, and the error in the determination of the corresponding positions and thermal factors is huge. For this reason, a combined refinement from NPD and XRD data was essential to accurately determine the 4*f* and 4*h* positions. The wavelength of the neutrons was refined to 1.4930(6) Å. The lattice parameters and the discrepancy factors obtained in the refinement are presented in Table 1. In Table 2, the atomic positions and the occupancy of the Mn/Cr cations are shown. A list of selected atomic distances and angles is shown in Table 3. The goodness of the fit of the NPD data is displayed in Fig. 2a. The second series of Bragg reflections corresponds to vanadium from the double-walled sample holder.

The neutron diffraction pattern collected at $T = 5$ K did not contain any additional information, extra peaks, or additional intensity on low-angle Bragg reflections that could be attributed to the establishment of a long-range ordered magnetic structure. The pattern collected with a longer wavelength, $\lambda = 1.886$ Å, could be perfectly refined by considering the crystal structure alone. The lattice parameters and discrepancy factors, atomic positions and

Table 1
Lattice parameters and reliability factors after the Rietveld refinements from combined NPD ($\lambda = 1.494$ Å) and XRD data at 295 K, and NPD ($\lambda = 1.886$ Å) at 5 K.

T (K)	295	5
a (Å)	7.2617(6)	7.2425(5)
b (Å)	8.5161(6)	8.5136(5)
c (Å)	5.7126(5)	5.7078(4)
V (Å^3)	353.28(5)	352.11(4)
χ^2	1.98	2.15
R_p (%)	1.21	1.56
R_{wp} (%)	1.54	1.97
R_{exp} (%)	1.10	1.34
R_{Bragg} (%)	5.98	7.58

Table 2
Atomic parameters after the refinement of the crystallographic structure from combined NPD ($\lambda = 1.494$ Å) and XRD data at 295 K, and NPD ($\lambda = 1.886$ Å) at 5 K.

T (K)	295	5
Dy 4*g* (x, y, 0)		
x	0.1383(4)	0.1379(3)
y	0.1721(3)	0.1722(3)
B (Å^2)	0.47(4)	0.45(5)
(Cr, Mn) 4*f* (0,1/2,z)		
z	0.2508(5)	0.2508(5)
B (Å^2)	0.3	0.3
Occup. (%)	0.44(1)/0.56(1)	0.44(1)/0.56(1)
(Mn, Cr) 4*h* (x,y,1/2)		
X	0.4013(3)	0.4013(3)
y	0.3559(3)	0.3559(4)
B (Å^2)	0.3	0.3
Occup. (%)	0.38(1)/0.62(1)	0.38(1)/0.62(1)
O1 4*e* (0,0,z)		
z	0.277(1)	0.276(1)
B (Å^2)	0.57(10)	0.85(13)
O2 4*g* (x,y,0)		
x	0.1671(11)	0.1655(10)
y	0.4430(8)	0.4428(7)
B (Å^2)	1.18 (13)	0.94(13)
O3 4*h* (x,y,1/2)		
x	0.1560(11)	0.1545(10)
y	0.4296(9)	0.4289(7)
B (Å^2)	0.96(12)	0.87(13)
O4 8*i* (x,y,z)		
x	0.3936(6)	0.3958(6)
y	0.2093(5)	0.2079(5)
z	0.2470(8)	0.2429(7)
B (Å^2)	0.68(8)	1.22(9)

Table 3
Main bond distances (Å) and selected angles (deg°) for $DyCrMnO_5$ at 295 and 5 K.

T (K)	295	5
$Dy^{3+}O_8$		
Dy–O1 (x2)	2.378(5)	2.371(5)
Dy–O2	2.316(7)	2.312(6)
Dy–O2	2.409(8)	2.417(7)
Dy–O4 (x2)	2.351(5)	2.347(5)
Dy–O4 (x2)	2.484(5)	2.458(5)
⟨Dy–O⟩	2.394	2.383
$(Cr, Mn)^{4+}O_6$		
M–O2 (x2)	1.939(5)	1.929(5)
M–O3 (x2)	1.916(5)	1.908(5)
M–O4 (x2)	1.943(4)	1.925(4)
⟨M–O⟩	1.929	1.920
$(Mn, Cr)^{3+}O_5$		
M'–O1 (x2)	1.910(5)	1.929(5)
M'–O3	1.889(8)	1.908(5)
M'–O4 (x2)	1.911(4)	1.925(4)
⟨M'–O⟩	1.906	1.920
M–M	2.8651(3)	2.8627(2)
M–M	2.8475(2)	2.8451(2)
M'–M'	2.8422(2)	2.8397(1)
M'–O1–M'	96.2(2)	95.9(2)
M–O2–M	95.3(2)	95.8(2)
M–O3–M	96.0(2)	96 .4(2)
M–O3–M'	131.4(3)	131.1 (3)
M–O4–M'	125.4(2)	125.0 (2)

the most important atomic distances and bonding angles are also included in Tables 1–3. As can be observed in Table 2, the antisite disorder between the Cr and Mn cations was fixed to those found at room temperature. The experimental and calculated NPD patterns are compared in Fig. 2b.

The calculation of the bond-valence sums allowed us to have an estimation of the valences of the cations in both positions at room temperature. The bond-valence sum (V_i) is calculated as $V_i = \Sigma_j S_{ij}$, where S_{ij} is the bond valence between the ith and jth atoms and it is defined as $S_{ij} = \exp[(d_0 - d_{ij})/0.37]$ [19]; d_{ij} is the bond length between the ith and jth atoms and d_0 the bond-valence parameter. The determined valences are 3.74(3)+ for the cations in the octahedral position and 3.11(3)+ for the cations in the pyramidal position, which justify our assumption that Mn and Cr cations at the octahedral positions exhibit a tetravalent oxidation state, whereas the metals at the pyramidal positions are trivalent, as required to preserve the electroneutrality of this oxide.

Fig. 3 shows a projection of the crystallographic structure along the c-axis. The different oxygen coordinations of the metal atoms occupying the 4*f* and 4*h* sites are highlighted: whereas at the 4*f* site, the $(Cr, Mn)^{4+}$ ions are six-fold coordinated in $M^{4+}O_6$ distorted octahedra, the $(Mn, Cr)^{3+}$ ions at the 4 h site are inside the $M^{3+}O_5$ distorted tetragonal pyramids. Given the large level of antisite disordering observed for this oxide, also comparable to that described for $YCrMnO_5$ [16], the octahedral 4*f* positions are about half occupied by Cr and Mn, whereas the pyramidal 4*h* sites are about two thirds occupied by Mn, given the suitability of this irregular environment for the Jahn–Teller Mn^{3+} cation. In the crystal structure (Fig. 3), there are dimer units M'_2O_{10} constituted by two pyramids sharing edges via O1 oxygen atoms. On the other hand, $M^{4+}O_6$ octahedra share edges via O2 and O3 oxygens, forming infinite chains running along the c-axis. Neighboring chains are interconnected through the M'_2O_{10} pyramidal dimer units via O3 and O4 oxygen atoms.

3.3. Magnetic measurements

The ZFC and FC curves of the *dc* susceptibility are presented in Fig. 4. Both curves almost coincide in the entire range of temperatures measured, only at very low temperatures the curves slightly diverge. The susceptibility smoothly increases on cooling without showing any significant anomaly, which suggests the absence of a long-range magnetic ordering effect. The reciprocal susceptibility data (inset of Fig. 4) show a subtle kink at ~140 K,

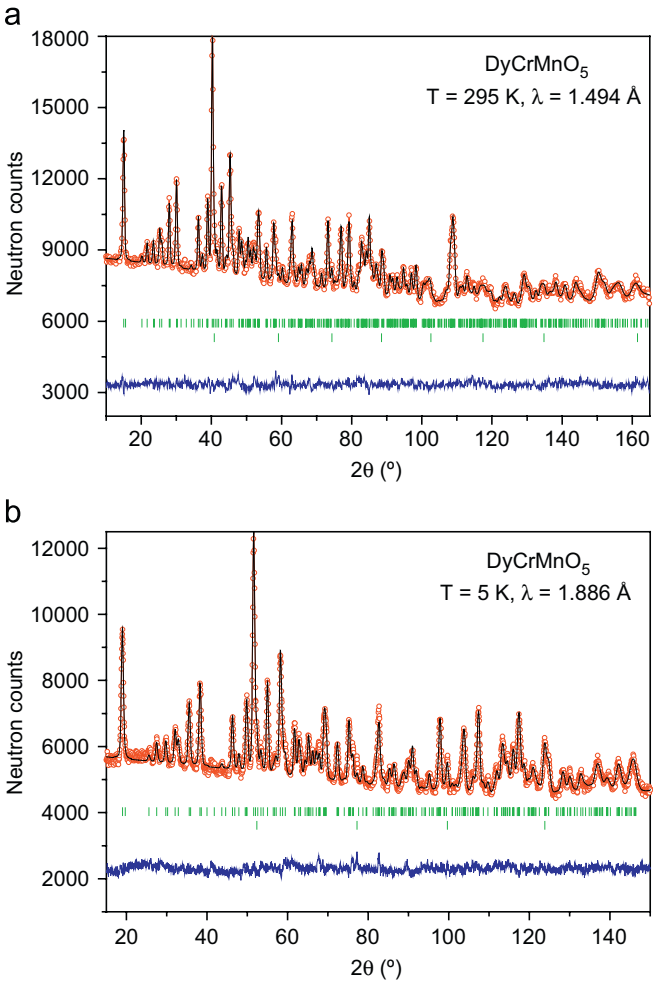

Fig. 2. Comparison of the observed (circles), calculated (solid line), and difference (at the bottom) NPD patterns. The two series of tick marks correspond to the positions of the allowed Bragg reflections for the main phase and vanadium at temperature (a) $T = 295$ and (b) 5 K.

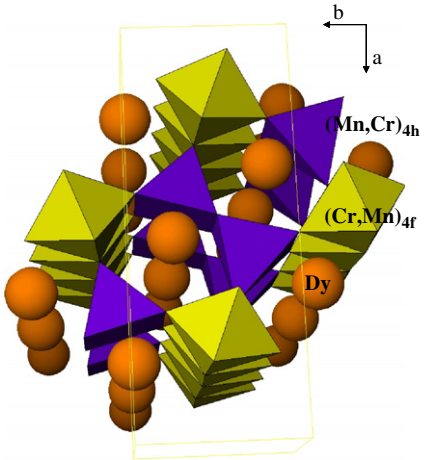

Fig. 3. View of the crystallographic structure of $DyCrMnO_5$ along the *c*-axis. Octahedra and tetragonal pyramids correspond to $(Cr,Mn)^{4+}O_6$ and $(Mn,Cr)^{3+}O_5$ polyhedra. The octahedra share edges, forming infinite chains along the *c*-axis. The pyramids form dimer units, linking together the chains of octahedra. The spheres represent the Dy atoms.

which could indicate the onset of short-range magnetic interactions that do not give rise to the establishment of a magnetic structure, given the large degree of antisite disordering and,

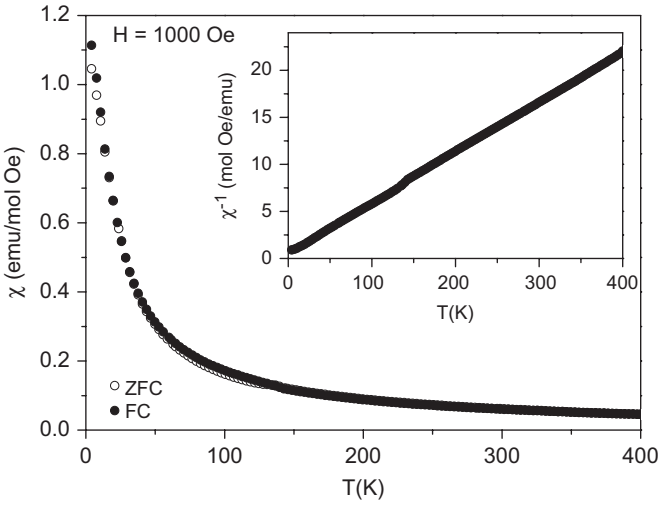

Fig. 4. Thermal evolution of the field cooling (FC) and zero-field cooling (ZFC) *dc* susceptibility. Upper inset: reciprocal susceptibility (ZFC data).

hence, magnetic frustration present in this compound. The $1/\chi$ can be fitted to a Curie–Weiss law (goodness of the fit $R = 0.9998$), giving a paramagnetic temperature $\Theta_{Weiss} = -16.90(2)$ K, suggesting the presence of weak antiferromagnetic interactions. The value of the effective paramagnetic moment $\mu_{eff} = 12.316(5)\,\mu_B$/f.u. can be compared with the theoretical magnetic effective magnetic moment for the crystallographic formula $Dy[Mn_{0.44(1)}Cr_{0.56(1)}]^{4+}[Cr_{0.38(1)}Mn_{0.62(1)}]^{3+}O_5$, by considering the expression $\mu_{eff} = (0.44\,\mu(Mn^{4+})^2 + 0{\cdot}56\,\mu(Cr^{4+})^2 + 0.38\,\mu(Cr^{3+})^2 + 0.62\,\mu(Mn^{3+})^2 + \mu(Dy^{3+})^2)^{1/2}$; the effective magnetic moments for spin-only Mn^{4+}, Mn^{3+}, Cr^{4+}, Cr^{3+}, and Dy^{3+} ($^6H_{15/2}$ ground state configuration) are 3.87, 4.90, 3.87, 2.83, and 10.63 μ_B, respectively, which implies an effective magnetic moment of 12.02 μ_B, in excellent agreement with the experimental value.

In the isothermal magnetization curves displayed in Fig. 5, a narrow hysteresis loop (coercive field = 470 Oe) is observed at $T = 5$ K with a maximum magnetization of 5.11 μ_B/f.u. reached for the maximum applied field of 50 kOe. At 50, 100, and 300 K the isothermal magnetization curves present a linear behavior, corresponding to a paramagnetic state.

4. Discussion

It can be considered that $DyCrMnO_5$ is derived from the parent $DyMn_2O_5$ oxide (containing one Mn^{3+} and one Mn^{4+} cation per formula) by replacing, nominally, half the Mn atoms by Cr atoms. In fact, $DyCrMnO_5$ is isostructural to RMn_2O_5 oxides, as expected from the comparable ionic sizes for Cr^{3+} and Mn^{3+} (0.615 and 0.645 Å, respectively), and Mn^{4+} and Cr^{4+} (0.53 and 0.55 Å, respectively), in six-fold coordination and high-spin state for both cations [20]. The unit-cell volume for $DyMn_2O_5$, 354.91 Å^3 [21], is slightly larger than for $DyCrMnO_5$, 353.28(5) Å^3. Some distinctive features have been found in the bonding distances of the $Mn^{4+}O_6$, $Cr^{3+}O_5$, and $Dy^{3+}O_8$ polyhedra. Regarding the $Mn^{4+}O_6$ octahedra the changes are little significant; the average bonding distance value is 1.918(2) Å in $DyMn_2O_5$ and 1.929 Å in $DyCrMnO_5$. In both cases the $Mn^{4+}O_6$ octahedra are flattened, with three pairs of Mn–O distances; the Mn–O3 and Mn–O4 bonds in the equatorial plane correspond to the shorter and longer distances, respectively. Regarding the tetragonal pyramids, $(Mn, Cr)^{3+}O_5$, the equatorial (Mn, Cr)–O1 and (Mn, Cr)–O4 bond distances (forming the square basis of the pyramid) are similar to the corresponding Mn–O distances in the $Mn^{3+}O_5$ units of the RMn_2O_5 compounds,

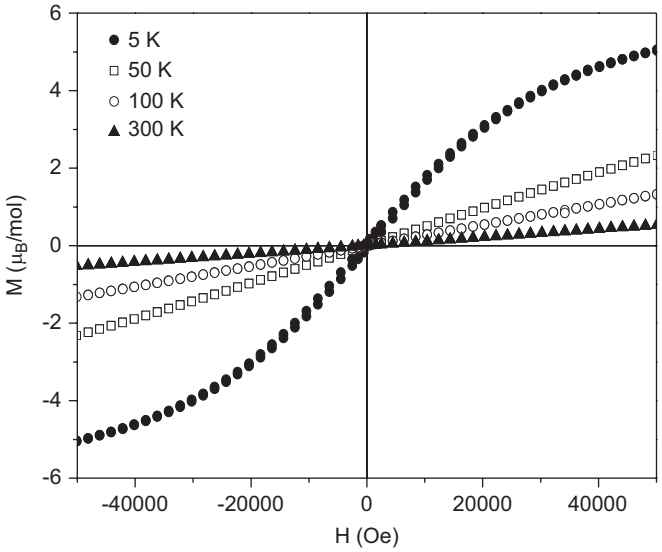

Fig. 5. Magnetization vs magnetic field isotherms at $T = 3$, 50, 100, and 300 K.

whereas the axial (Mn, Cr)–O3 bond length (1.889(8) Å) is shorter than that observed in $DyMn_2O_5$, where the Mn^{3+}–O3 bond in the axial position is the longest one in the $Mn^{3+}O_5$ pyramid (2.020(5) Å). This is probably related to the Jahn–Teller character of Mn^{3+} cations, favoring an increase of the axial bond lengths in the $Mn^{3+}O_5$ pyramids, in contrast with the non-Jahn–Teller character of Cr^{3+} ($3d^3$ configuration). A similar feature (flattened (Mn, Cr)O_5 pyramid) was found in the closely related $YCrMnO_5$ oxide [16]. With respect to the oxygen coordination of Dy^{3+} cations, it can be described as $Dy^{3+}O_8$ bicapped prisms, with average $\langle$Dy–O$\rangle$ distances of 2.394 Å, in good agreement with the $\langle$Dy–O$\rangle$ bond lengths of 2.389 Å observed in $DyMn_2O_5$.

The high level of antisite disordering exhibited by $DyCrMnO_5$ is noteworthy. The octahedral positions are occupied by roughly 50% of Mn and Cr cations, and the pyramidal groups contain two thirds of Mn and one third of Cr cations. A neutron diffraction study was essential to determine this feature, owing to the contrasting neutron scattering lengths of Cr and Mn. Conversely, in RFeMnO_5 (R = Dy, Ho, Er, Y) [12,13,15,22], a clear preference of Mn^{4+} for the octahedral positions and Fe^{3+} for the tetrahedral sites was observed. We suggest that this difference could arise from the relative ease of oxidation of Cr vs Fe to reach the tetravalent oxidation state required to incorporate into the octahedral positions, which is feasible under the high-pressure conditions utilized in the synthesis of this compound.

The magnetic properties of $DyCrMnO_5$ are dramatically influenced by the Cr/Mn antisite disordering. The susceptibility vs temperature curve of $DyCrMnO_5$ does not suggest the establishment of a long-range magnetic structure even at low temperatures. The random distribution of Cr and Mn cations over the octahedral and pyramidal positions, in the mixed valences Cr^{3+}/Cr^{4+} and Mn^{4+}/Mn^{3+}, which implies the incorporations of both cations into both positions, seems to hinder the establishment of a long-range ferrimagnetic ordering between both magnetic sublattices. For the same reason, the NPD technique does not provide any signal of magnetic ordering, since the reflections do not shows any magnetic contribution.

The curves of magnetization vs field show a subtle hysteretic behavior at 5 K with a non-negligible saturation magnetization of 5.11 μ_B/f.u. for the higher applied field of 50 kOe. We believe that this is due to the polarization of the Dy^{3+} moments under an external magnetic field, in the absence of which the Dy^{3+} moments remain in a quasi-paramagnetic state, as shown by neutron diffraction, since the internal polarization by the molecular field of the Cr^{3+} and Mn^{4+} sublattices remains very weak even at low temperatures. Therefore, it is clear that the weak direct superexchange interaction between the Dy^{3+} cations via the Dy^{3+}–O1–Dy^{3+}, Dy^{3+}–O2–Dy^{3+}, and Dy^{3+}–O4–Dy^{3+} paths is very weak. At low temperatures, Cr and Mn cations are involved in short-range antiferromagnetic interactions (as indicated by the Weiss temperature), little sensitive to an external magnetic field despite lacking long-range coherence to establish a magnetic structure; we believe that the polarization observed in Fig. 5 at 5 K comes mainly from Dy^{3+} moments. In other related compounds containing strongly paramagnetic rare-earth cations, such as RFeMnO_5 (R = Er, Ho, Dy) [12,15,22], it has been shown that the rare-earth moment is strongly polarized and takes part of the low-temperature magnetic structure; in the present case the lack of any measurable magnetic order in the (Mn, Cr) sublattices accounts for the paramagnetic state of the Dy^{3+} moments in the absence of an external magnetic field.

5. Conclusions

A new compound has been obtained by partially replacing Mn by Cr in the parent $DyMn_2O_5$ oxide. The crystallographic structure of $DyCrMnO_5$ is isotypic with that of RMn_2O_5 materials (space group *Pbam*), and contains chains of edge-linked $(Mn, Cr)^{4+}O_6$ octahedra connected by dimer groups of square pyramids $(Cr, Mn)^{3+}O_5$. A peculiar structural feature is that the square pyramids of the Cr compound are not elongated, showing shortened axial distances relative to the $Mn^{3+}O_5$ pyramids in $DyMn_2O_5$. A high degree of antisite disordering has been found over the 4*f* and 4*h* sites, ideally occupied by the Mn^{4+} and Cr^{3+}, respectively. The low-temperature NPD patterns do not show any magnetic contribution, indicating that long-range magnetic ordering is not established down to low temperature, although the Dy^{3+} magnetic moments are susceptible to be polarized by an external magnetic field at the lowest temperature of 5 K.

Acknowledgments

We thank the financial support of the Spanish Ministry of Education to the project MAT2007-60536. This work was partially performed at the spallation source SINQ, Paul Scherrer Institute, Villigen, Switzerland.

References

[1] W. Eerenstein, N.D. Mathur, J.F. Scott, Nature London 442 (2006) 17.
[2] L.C. Chapon, G.R. Blake, M.J. Gutmann, S. Park, N. Hur, P.G. Radaelli, S.W. Cheong, Phys. Rev. Lett. 93 (2004) 177402.
[3] T. Kimura, T. Goto, H. Shintani, K. Ishizaka, T. Arima, Y. Tokura, Nature London 426 (2003) 6.
[4] A.F. García-Flores, E. Granado, H. Martinho, R.R. Urbano, C. Rettori, E.I. Golovenchits, V.A. Sanina, S.B. Oseroff, S. Parkand, S.-W. Cheong, Phys. Rev. B 73 (2006) 104411.
[5] M. Tachibana, K. Akiyama, H. Kawaji, T. Atake, Phys. Rev. B 72 (2005) 224425.
[6] Y. Noda, Y. Fukuda, H. Kimura, I. Kagomiya, S. Matumoto, K. Kohn, T. Shobu, N. Ikeda, J. Kor. Phys. Soc. 42 (2003) S1192.
[7] S. Quezel-Ambrunaz, E.F. Bertaut, G.C. Buisson, R. Acad. Sci. 258 (1964) 3025.
[8] E.F. Bertaut, G. Buisson, A. Durif, A. Mareschal, M.C. Montmory, S. Quezel-Ambrunaz, Bull. Soc. Chim. Fr. (1965) 1132.
[9] J.A. Alonso, M.T. Casais, M.J. Martínez-Lope, J.L. Martínez, M.T. Fernández-Díaz, J. Phys.: Condens. Matter 9 (1997) 8515.
[10] G. Buisson, Phys. Status Solidi A 16 (1973) 533.
[11] G. Buisson, Phys. Status Solidi A 17 (1973) 191.
[12] A. Muñoz, J.A. Alonso, M.T. Casais, M.J. Martínez-Lope, J.L. Martínez, M.T. Fernández-Díaz Eur, J. Inorg. Chem. (2005) 685.
[13] A. Muñoz, J.A. Alonso, M.J. Martínez-Lope, J.L. Martínez, Chem. Mater. 16 (2004) 4087.

[14] A. Muñoz, J.A. Alonso, M.J. Martínez-Lope, J.L. Martínez, Eur. J. Inorg. Chem. (2007) 1972.
[15] A. Muñoz, J.A. Alonso, M.J. Martínez-Lope, J.L. Martínez, Phys. Rev. B 72 (2005) 184402.
[16] J.A. Alonso, M.J. Martínez-Lope, M.T. Casais, J.L. Martínez, V. Pomjakushin, Eur. J. Inorg. Chem. (2005) 2600.
[17] H.M. Rietveld, J. Appl. Crystallogr. 2 (1969) 65.
[18] J. Rodríguez-Carvajal, Physica B 192 (1993) 55.
[19] N.E. Brese, M. O'Keefe, Acta Crystallogr. B 47 (1991) 192.
[20] R.D. Shannon, Acta Crystallogr. A 32 (1976) 751.
[21] S.C. Abrahams, J.L. Bernstein, J. Chem. Phys. 46 (10) (1967) 3776.
[22] M.J. Martínez-Lope, M. Retuerto, J.A. Alonso, V. Pomjakushin, J. Solid State Chem. 181 (9) (2008) 2155.